

Systematic Physical Characterization of the γ -Ray Spectra of 2FHL Blazars

Jabus van den Berg^{1,2}, Markus Böttcher¹, Alberto Domínguez³ and Marcos López-Moya³

on behalf of the Fermi-LAT Collaboration

¹ Centre for Space Research, North-West University, Potchefstroom, South Africa

Markus.Böttcher@nwu.ac.za

² South African National Space Agency, Hermanus, South Africa

³ Grupo de Altas Energías, Universidad Complutense de Madrid, Madrid, Spain

NWU **Centre for Space Research**

van den Berg, J.P., Böttcher, M., Domínguez, A. & López-Moya, M. 2019, ApJ, 874, 47

Abstract

We test different physically motivated models for the spectral shape of the γ -ray emission in a sample of 128 blazars with known redshifts detected by Fermi-LAT at energies above 50 GeV. The first nine years of LAT data in the energy range from 300 MeV to 2 TeV are analyzed in order to extend the spectral energy coverage of 2FHL blazars in our sample. We compare these spectral data to four leptonic models for the production of gamma-rays through Compton scattering by a population of electrons with different spectral shapes. In the first three models we consider Compton scattering in the Thomson regime with different acceleration mechanisms for the electrons. In the fourth model we consider Compton scattering by a pure power law distribution of electrons with spectral curvature due to scattering in the Klein-Nishina regime. The majority of blazar γ -ray spectra are preferentially fit with either a power law with exponential cut-off in the Thomson regime or a power law electron distribution with Compton scattering in the Klein-Nishina regime, while a log-parabola with a low-energy power-law and broken power-law spectral shape in the Thomson regime appear systematically disfavoured, which is likely a consequence of the restriction to pure Thomson scattering which we imposed on those models. This finding may be an indication that the γ -ray emission from FSRQs in 2FHL is dominated by Compton scattering of radiation from the dusty torus, while in the case of BL Lac objects, it is dominated by synchrotron self-Compton radiation.

1 Background

Leptonic models of blazars assume that their high-energy x- and γ -ray emission are caused by inverse Compton scattering of low-energy photons by the same population of electrons which produced their low-energy synchrotron radiation (SR). The shape of the γ -ray spectrum is related to the energy distribution of the accelerated electrons, with a straightforward relation in the case of Compton scattering in the Thomson regime, but a more complex correlation in the Klein-Nishina regime [Böttcher et al., 2012; Dermer & Menon, 2012]. If the target photons originate from the co-spatially produced SR (typically peaking in the infrared, IR, to optical in the co-moving frame, leading to synchrotron self-Compton, SSC, emission) or from a dusty torus around the central accretion flow (peaking in the IR, leading to external Compton on dust torus emission), then the Compton scattering to GeV γ -ray energies typically occurs in the Thomson regime. If the target photons originate externally from the Broad Line Region (dominated by optical to ultraviolet photons in the AGN's stationary frame, leading to external Compton on BLR emission), then the Compton scattering to GeV energies typically occurs in the Klein-Nishina regime. A deviation of the γ -ray spectra of blazars from a pure power-law may thus be caused either by an underlying electron population that deviates from a pure power-law due to some acceleration mechanism, and/or by the transition of the Compton scattering process from the Thomson to the Klein-Nishina regime.

2 Blazar Sample

Our sample includes all 128 blazars from 2FHL [Ackermann et al., 2016].

- First 9 years of Fermi-LAT data (450 weeks, from MJD 56048 to MJD 57772)
- Extended energy range from 300 MeV to 2 TeV
- Redshifts range from $z = 0.004283$ (M87) to $z = 2.1$ (MG4 J00800+4712), with the median of the distribution at $z = 0.215$

The blazar population:

- 106 BL Lacs
- 10 flat-spectrum radio quasars (FSRQs)
- 12 other types of AGN (blazars of uncertain type, radio galaxies, other AGN)

Blazar classification according to synchrotron peak frequency:

- 33 low-synchrotron peak (LSP)
- 12 intermediate-synchrotron peak (ISP)
- 82 high-synchrotron peak (HSP)
- 1 without clear classification

Blazar classification according to variability (we used the variability analysis of 3FHL [Ajello et al., 2017] for its extended energy range):

- 47 variable
- 81 assumed to be non-variable

3.1 Thomson Regime Models

Here the turnover in the spectra is caused by the electron distributions.

Assumptions:

- Differential Compton cross section approximated by delta function.
- Isotropic electron and target photon distributions.
- Narrow target photon distribution is mono-energetic in comparison with the electron distribution.
- Relativistic electrons.

3.1.1 Radiation-reaction-limited first-order Fermi acceleration

Power-law with exponential cut-off (PL+EC) electron distribution, yielding

$$\nu F_\nu = C_1 \nu^{-\alpha+1} \nu_0^\alpha \exp\left(-\sqrt{\frac{\nu}{\nu_c}}\right) \quad (1)$$

where ν is the frequency, C_1 is an arbitrary proportionality constant, ν_0 is the target photons' frequency, $\alpha = (\rho - 1)/2$ is the spectral index, with ρ the electron distribution's spectral index, and $\nu_c = \gamma_c^2 \nu_0$ is the cut-off frequency, with γ_c the electron distribution's cut-off Lorentz factor (notice the degeneracy between ν_c and ν_0).

3.1.2 Stochastic acceleration with continuous injection

Log-parabolic (LP+PL) electron distribution with continuous injection (low-energy power-law), yielding

$$\nu F_\nu = C_2 \nu \sqrt{\frac{\nu}{\nu_0}} \begin{cases} (\nu/\nu_b)^{-a/2} & \text{if } \nu \leq \nu_b \\ (\nu/\nu_b)^{-[a+b \ln(\nu/\nu_b)/2]/2} & \text{if } \nu > \nu_b \end{cases} \quad (2)$$

where a is the low-energy limit of the slope, b parametrizes the curvature, and $\nu_b = \gamma_b^2 \nu_0$ is the transition frequency from the low-frequency power-law to the log-parabola, with γ_b the corresponding Lorentz factor of the electron distribution (notice the degeneracy between ν_b and ν_0). See Massaro et al. [2004] and Tramacere et al. [2007, 2011] for discussions on stochastic acceleration explaining the low-energy synchrotron peak of BL Lacs.

3.1 Thomson Regime Models (Continued...)

3.1.3 First-order Fermi acceleration with different acceleration/cooling regimes

Broken power-law (BPL) electron distribution, yielding

$$\nu F_\nu = C_3 \nu \sqrt{\frac{\nu}{\nu_0}} \begin{cases} (\nu/\nu_b)^{-q/2} & \text{if } \nu \leq \nu_b \\ (\nu/\nu_b)^{-s/2} & \text{if } \nu > \nu_b \end{cases} \quad (3)$$

where q and s are the spectral indexes of the low- and high-energy power laws, respectively (there is again a degeneracy between ν_b and ν_0).

3.2 Klein-Nishina Regime Model

Here the turnover in the spectra is caused by the decrease of the Compton cross section, even for a pure power-law electron distribution.

Assumptions:

- Differential Compton cross section approximated by the head-on approximation for ultra-relativistic electrons.
- Isotropic electron and target photon distributions.
- Narrow target photon distribution is mono-energetic in comparison with the electron distribution.
- Power-law electron distribution.

Formula of Jones [1968] for Compton scattering, including the Klein-Nishina (KN) regime,

$$\nu F_\nu = C_4 \frac{\epsilon^2}{\epsilon_0} \int_{\gamma_1}^{\infty} \left[2u \ln(u) + (1+2u)(1-u) + \frac{(1-u)(4\epsilon_0 \gamma_e u)^2}{2(1+4\epsilon_0 \gamma_e u)} \right] \frac{d\gamma_e}{\gamma_e^{p+2}} \quad (4)$$

where $\epsilon = h\nu/m_ec^2$ is the dimensionless energy, with h Planck's constant, m_e the electron mass, and c the speed of light, γ_e is the electron Lorentz factor, ϵ_0 is the dimensionless target photon energy, $\gamma_1 = (\epsilon + \sqrt{\epsilon^2 + \epsilon/\epsilon_0})/2$ is the lower integration limit resulting from the minimum Lorentz factor that can scatter the target photons to a given ϵ , and $u = \epsilon/4\epsilon_0 \gamma_e (\gamma_e - \epsilon)$.

4 Fitting Methodology

- Flux corrected for attenuation by extragalactic background light using the model of Domínguez et al. [2011].
- Models fitted with a χ^2 -minimization routine.

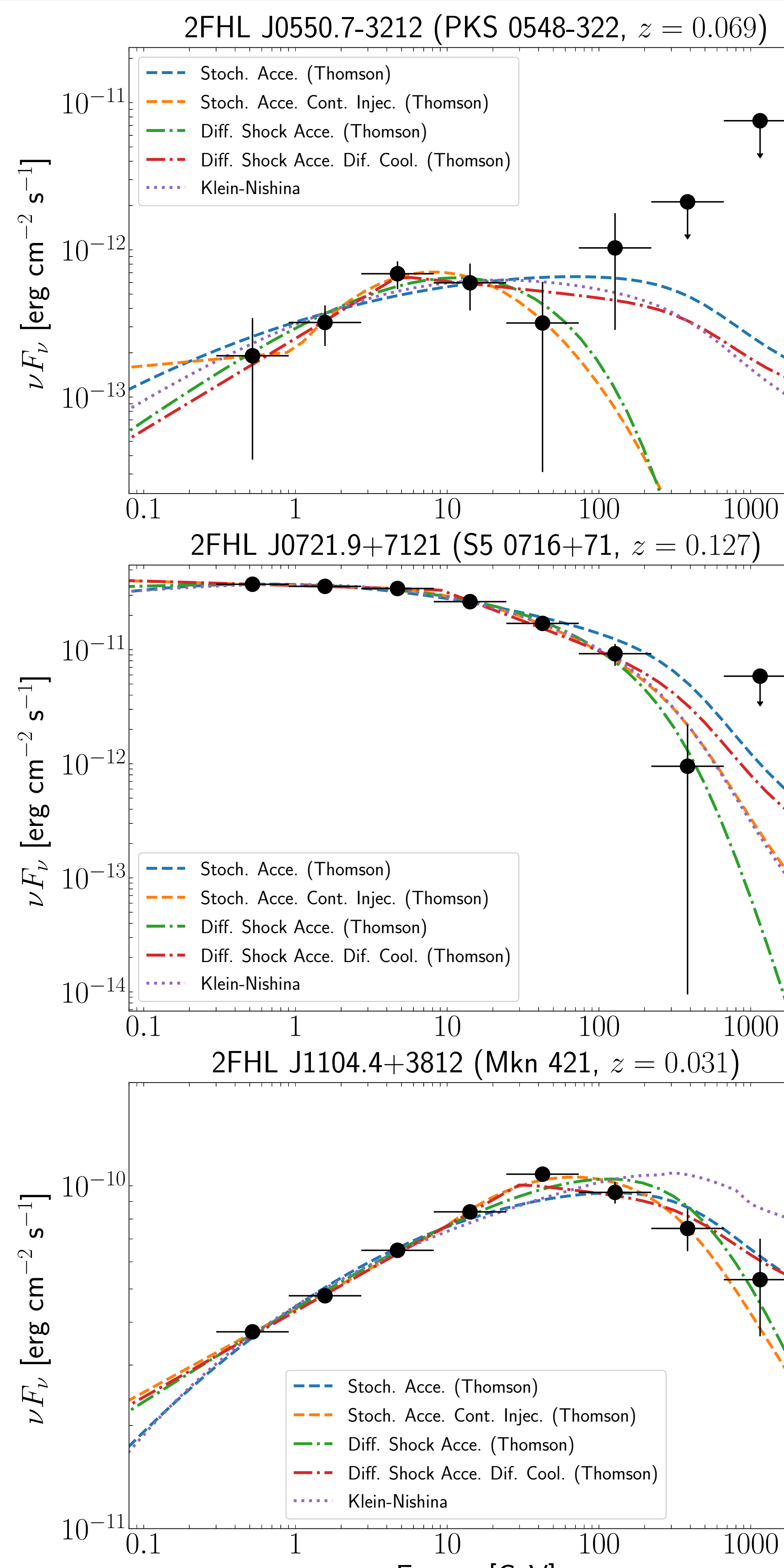


Fig. 1: Example high-energy SEDs of three sources in the sample. LAT data (black circles) are fitted with: stochastic acceleration with continuous injection in the Thomson regime (LP+PL, dashed-orange line), radiation-reaction-limited first-order Fermi acceleration in the Thomson regime (PL+EC, dash-dotted green line), radiation-reaction-limited first-order Fermi acceleration with different acceleration/cooling processes in the Thomson regime (BPL, dash-dotted red line), and first-order Fermi acceleration with Compton scattering in the Klein-Nishina regime (KN, dotted magenta line).

The apparent up-turn in the models at high energies are caused by transforming the models fitted to the intrinsic flux to the observed flux, due to the optical depth becoming almost constant at those energies for the given redshifts. The step-like feature of the Klein-Nishina model for Mkn 421 is due to the numerical evaluation of the integral.

5.1 Rejection Criteria

Parameters were not restricted during the fitting routine and hence, in some cases the best-fit parameters are problematic and/or unphysical.

A model fit was rejected due to:

- A statistically bad fit, i.e. when $Q < 0.001$ (Q is the probability for the χ^2 -value to be larger by chance).
- Negative curvature in the LP+PL model ($b < 0$ causes flux to increase at low and high energies).
- Spectra being too hard to reconcile with known particle acceleration mechanisms, i.e. when $\alpha < 0.5$, $a < 1$, $q < 2$, or $p < 1$.
- The high energy component of the BPL model being harder than the low energy component, i.e. when $s < q$.

5.2 Averages of Fitted Model Parameters (Only Accepted Fits)

Model	Parameter	All (128)	Variable (47)	Non-variable (81)
PL+EC	χ_r^2	1.4±0.8	1.3±0.8	1.5±0.9
	α	0.9±0.2	0.9±0.2	0.8±0.2
	ν_c [Hz] [†]	26±1	25±1	26±2
LP+PL	χ_r^2	2.0±1.3	2.0±1.2	2.0±1.5
	a	2.6±0.5	2.9±0.4	2.4±0.6
	b	0.5±0.7	0.3±0.2	0.6±0.9
BPL	ν_b [Hz] [†]	23.9±0.5	23.9±0.4	23.9±0.5
	χ_r^2	1.7±1.0	1.9±1.2	1.6±0.8
	q	2.8±0.5	2.9±0.5	2.6±0.4
KN	s	3.4±0.8	3.5±0.6	3.4±0.9
	ν_b [Hz] [†]	24.1±0.4	24.1±0.3	24.1±0.4
	χ_r^2	1.4±0.8	1.3±0.7	1.4±0.8
BL Lacs	p	2.1±0.3	2.2±0.3	2.0±0.3
	$\epsilon_0^†$	-5.3±0.6	-5.2±0.7	-5.3±0.6
	χ_r^2	1.4±0.8	...±...*	0.9±0.5
FSRQs	p	2.1±0.3	...±...*	1.9±0.3
	$\epsilon_0^†$	-5.3±0.6	...±...*	-5.5±0.7
	χ_r^2	1.4±0.8	1.5±0.8	1.2±1.1
Other	α	0.8±0.2	1.1±0.2	1.0±0.3
	ν_c [Hz] [†]	26±1	25±2	26±2
	χ_r^2	1.8±1.1	3.0±1.6	1.6±1.6
LP+PL	a	2.5±0.5	3.4±0.4	3.0±0.2
	b	0.5±0.8	0.3±0.2	0.2±0.1
	ν_b [Hz] [†]	24.0±0.5	23.6±0.2	23.9±0.2
BPL	χ_r^2	1.7±0.9	2.5±1.4	1.1±0.5
	q	2.7±0.4	3.5±0.4	3.1±0.3
	s	3.3±0.8	4.1±0.7	3.5±0.4
KN	ν_b [Hz] [†]	24.1±0.4	24.0±0.1	24.1±0.5
	χ_r^2	1.4±0.8	...±...*	0.9±0.5
	p	2.1±0.3	...±...*	1.9±0.3
No accepted model	$\epsilon_0^†$	-5.3±0.6	...±...*	-5.5±0.7

[†]Averages and standard deviations given for the base 10 logarithm of the parameters.

*No accepted model.

5.3 Best Fitting Model (Only Accepted Fits)

Models compared with likelihood ratio test at 95% confidence:

Model	All (128)	Variable (47)	Non-variable (81)